LITHOS 456–457 (2023) 107302

Contents lists available at ScienceDirect

LITHOS

journal homepage: www.elsevier.com/locate/lithos

Deciphering the sources and processes feeding young monogenetic volcanoes from the Michoacán Guanajuato Volcanic Field (Mexico): A study case of El Astillero and El Pedregal

Patricia Larrea [a,b,c,*], Elisabeth Widom [c], Claus Siebe [d], Sergio Salinas [e], Dave Kuentz [c]

[a] Department of Geology, Facultad de Ciencias Físicas y Matemáticas, Universidad de Chile, Plaza Ercilla 803, Santiago, Chile
[b] Andean Geothermal Center of Excellence (CEGA), FCFM, Universidad de Chile, Santiago, Plaza Ercilla 803, Chile
[c] Department of Geology & Environmental Earth Science, Miami University, Oxford, OH 45056, USA
[d] Departamento de Vulcanología, Instituto de Geofísica, Universidad Nacional Autónoma de México, Ciudad Universitaria, 04510 Coyoacán, Ciudad de México, Mexico
[e] Facultad de Ingeniería, División de Ingeniería en Ciencias de la Tierra, Universidad Nacional Autónoma de México, Ciudad Universitaria, 04510, Coyoacán, Ciudad de México, Mexico

ARTICLE INFO

Keywords:
Monogenetic volcanism
Holocene
Subduction zone
Mantle metasomatism
Crustal contamination
Trans-Mexican Volcanic Belt
Isotope systematics

ABSTRACT

El Astillero and El Pedregal monogenetic volcanoes formed ~500–700 CE in the Tancítaro region in the southern part of the Michoacán-Guanajuato volcanic field, only 25 km to the SW of the historic Paricutin volcano. The ~6-year-long eruption was characterized by a change from explosive to effusive activity, accompanied by a shift in the location of the active vents. Initial activity was Strombolian-explosive and first formed the El Astillero cone before turning effusive with the emission of several lava flows. Then, a new vent located 2 km to the ENE opened and produced the purely effusive (non-explosive) El Pedregal lava flow field. As the eruption progressed, the bulk magma composition (major and trace elements) changed from basaltic andesite to andesite (SiO_2 = 52–59 wt%), which is also reflected in a successive change in the petrography of the erupted tephras and lavas. However, the El Pedregal lava sequence shows small Mg# reversals followed by a marked final reversal to more mafic compositions. Likewise, $^{87}Sr/^{86}Sr$ (0.70388–0.70403), $^{143}Nd/^{144}Nd$ (0.512836–0.512742), $^{206}Pb/^{204}Pb$ (18.632–18.671), $^{207}Pb/^{204}Pb$ (15.583–15.598), $^{208}Pb/^{204}Pb$ (38.376–38.450), $^{176}Hf/^{177}Hf$ (0.28301–0.28290), and $^{187}Os/^{188}Os$ (0.1258–0.1865) isotope ratios changed systematically as the eruption progressed, and record a final shift to a distinct isotopic signature. The spatio-temporal proximity of both vents and the petrographic and geochemical characteristics of their magmas suggest a comagmatic evolution that can be explained by a combination of variable degrees of magma recharge, magma mixing, and fractional crystallization of subduction-modified mantle melts. A similar combination of magmatic processes for the genesis and evolution of these magmas has also been proposed for other young monogenetic volcanoes in the Michoacán-Guanajuato volcanic field (e.g., Paricutin, Jorullo, and the Tacámbaro cluster). Accordingly, primitive magmas in the Trans-Mexican Volcanic Belt are subduction-modified mantle melts that evolve largely by crystal fractionation and pass through the crust without significant assimilation.

1. Introduction

The Michoacán-Guanajuato Volcanic Field (MGVF) in the west-central part of the Trans-Mexican Volcanic Belt (TMVB; Fig. 1), is one of the largest volcanic fields in the world, characterized by a variety of volcanic styles and magma compositions (Hasenaka and Carmichael, 1985a, 1985b; Sosa-Ceballos et al., 2021; Torres-Sánchez et al., 2022; Valentine and Connor, 2015). The volcanic field covers an area of ~40,000 km^2 and hosts >1200 monogenetic vents formed since the Pliocene, including scoria cones, small-to-medium sized shields, phreatomagmatic craters, felsic domes, and fissural lava flows, as well as two extinct stratovolcanoes, Tancítaro and Patambán (e.g., Chevrel et al., 2016; Guilbaud et al., 2012; Kshirsagar et al., 2015; Mahgoub et al., 2017a, 2017b, 2018; Osorio-Ocampo et al., 2018; Ownby et al., 2011; Pola et al., 2014; Torres-Sánchez et al., 2022). Volcanic activity in the MGVF started in the Pliocene with a magmatic flux of ~800 km^3/Ma

* Corresponding author at: Departamento de Geología, Facultad de Ciencias Físicas y Matemáticas, Universidad de Chile, Plaza Ercilla 803, Santiago, Chile.
E-mail address: patricia.larrea@uchile.cl (P. Larrea).

https://doi.org/10.1016/j.lithos.2023.107302
Received 28 March 2023; Received in revised form 24 July 2023; Accepted 26 July 2023
Available online 29 July 2023

(Hasenaka and Carmichael, 1985b). Moreover, according to available information, its activity increased from the Pleistocene through the Holocene, with an eruptive recurrence interval in the past 40 ka of ~2 × 10^{-3} eruptions per year, which is significantly higher than the long-term Quaternary average of ~4 × 10^{-4} eruptions per year (Hasenaka and Carmichael, 1985b; Valentine and Connor, 2015). Remarkably, at least 30 volcanoes are younger than 25,000 y BP, including the historic Jorullo (1759–1774) and Paricutin (1943–1952) volcanoes (e.g., Guilbaud et al., 2011; Larrea et al., 2017; Luhr and Simkin, 1993; Rasoazanamparany et al., 2016). The repeated seismic swarms that have been registered in the Paricutin area in recent decades (e.g., Legrand et al., 2023) further underscore that the MGVF remains potentially active and that a new eruption should be expected in the future.

The large extent of magmatism over the wide MGVF area beneath a ~ 40-km-thick continental crust seems to be controlled by its tectonic configuration (Carmichael, 2002; Gómez-Vasconcelos et al., 2020; Kim et al., 2012); the MGFV occurs in an extensional tectonic setting related to the oblique convergence and near-horizontal position of the subducting Cocos plate relative to the North America plate. In addition, the recent identification of Holocene and Pleistocene clusters, consisting of several monogenetic volcanoes grouped both in space and time within the MGVF, suggests a close petrogenetic relationship. The volcanoes forming each cluster erupted in a geologically short sequence (separated by time intervals of hundreds to a few thousands of years) within small areas of few tens of square kilometers. Clusters identified so far include Queréndaro (Gómez-Vasconcelos et al., 2020), Tacámbaro (Guilbaud

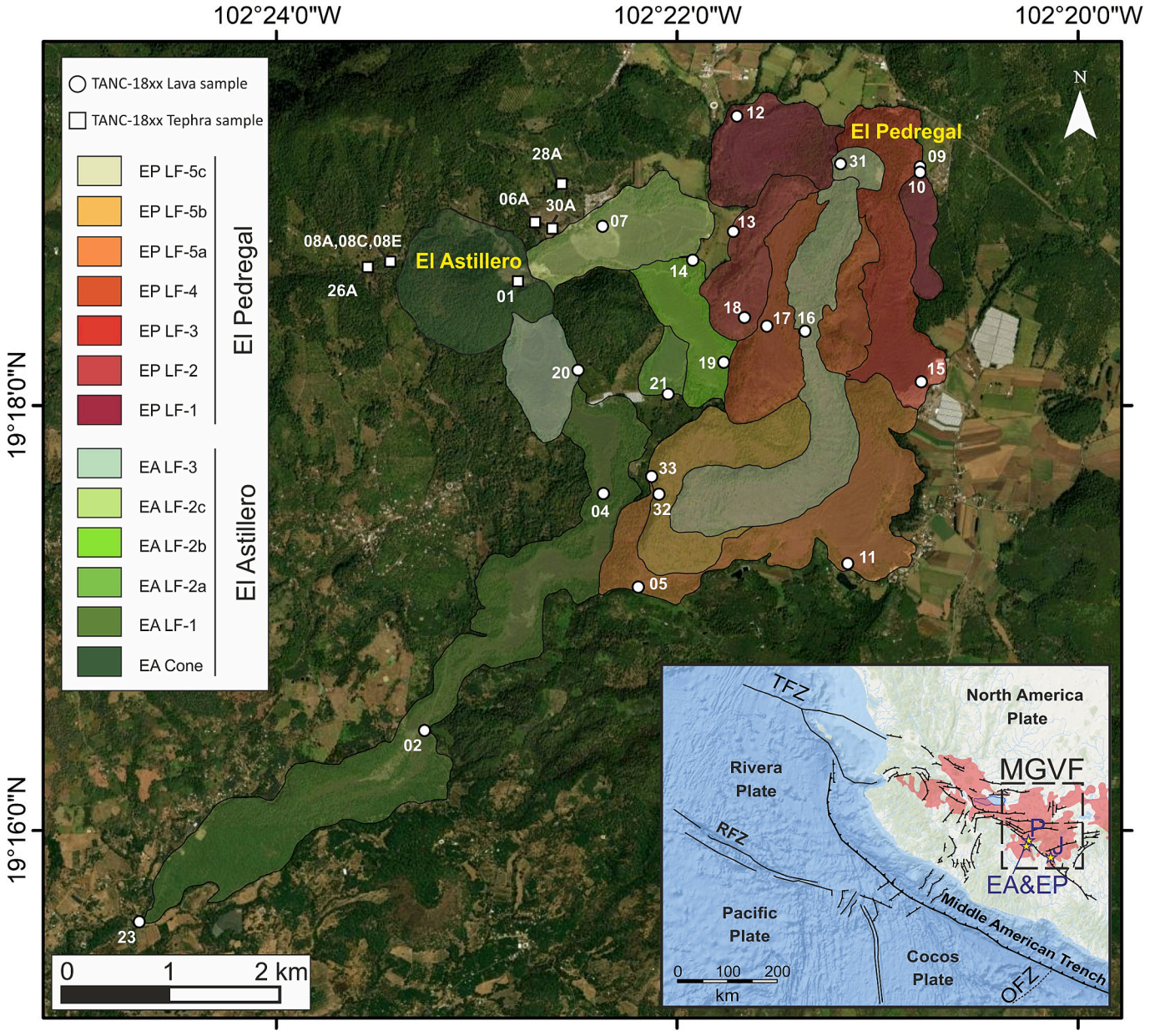

Fig. 1. Geological map of the El Astillero and El Pedregal volcanoes showing the emplacement sequence of lava flows as defined by Larrea et al. (2019a). Sampling locations of rocks analyzed in this study: lavas (circles) and tephras (squares). Note that sample numbers have been shortened to the last two identification digits (e.g., TANC-1801 is referred as 01); see Appendix B - Table B.1 for sample coordinates and chemical compositions. This map was created using ArcGIS® software by Esri ArcGIS® and ArcMap™. Inset map shows the main tectonic features of SW Mexico with the location of the Trans-Mexican Volcanic Belt (reddish polygon), and the Michoacán-Guanajuato Volcanic Field (MGVF). Major fracture zones: Tamayo Fracture Zone (TFZ), Rivera Fracture Zone (RFZ), and Orozco Fracture Zone (OFZ). Volcanoes (yellow stars): EA = El Astillero, EP = El Pedregal, J = Jorullo, P=Paricutin. (For interpretation of the references to colour in this figure legend, the reader is referred to the web version of this article.)

et al., 2012, 2019; Mahgoub et al., 2017a), and Zacapu (Mahgoub et al., 2018; Reyes-Guzmán et al., 2018). In this context, Larrea et al. (2019a) proposed that the El Astillero and El Pedregal volcanoes might potentially represent the initial eruptions of an incipient cluster, i.e. a cluster that is still in the making.

Recent petrogenetic studies of the historic Paricutin and Jorullo eruptions have demonstrated that the magmatic processes controlling the formation and evolution of monogenetic volcanoes are far from simple (e.g., Larrea et al., 2019b, 2021; Rasoazanamparany et al., 2016). In addition, the occurrence of clustered monogenetic volcanism within the MGFV leads to several questions in regard to the processes that govern the formation and emplacement of magmas in close spatio-temporal proximity: What is the main mechanism of magma generation? What magmatic processes control the evolution of these clusters? Does crustal assimilation play a role? Are the volcanic vents that form a cluster related to the same magma batch or different independent magma batches?

In this work we aim to decipher some of the questions posed above based on the case of the ~500–700 CE El Astillero and El Pedregal monogenetic volcanoes, located near the towns of Tancítaro and Zirimbo, and only 25 km to the SW of Paricutin volcano (Fig. 1). We investigate the whole-rock geochemical variation of the eruptive sequence with time for major, trace, and Sr-Nd-Pb-Hf-Os isotopes (Fig. 2), and compare them with the Paricutin and Jorullo historic eruptions. Furthermore, we evaluate the magmatic processes that allowed these magmas to be emplaced in close temporal and spatial proximity, and discuss the roles of crustal assimilation, mantle source heterogeneity, and open-system processes in the evolution of these monogenetic centers.

2. Geological background and previous studies

El Astillero (N 19°18′34.34″ N, 102°22′57.24″ W, 2230 m.a.s.l.) and El Pedregal (N 19°19′07.08″ N, 102°21′04.56″ W, 2137 m.a.s.l.) volcanic centers formed in the southern part of the MGVF during the Late Holocene, approximately between 500–700 CE, as determined by paleomagnetic and radiocarbon dating (Larrea et al., 2019a; Fig. 1). This area comprises the ~4400 km^2 Tancítaro-Nueva Italia volcanic region (Ownby et al., 2011), which is constituted by >300 volcanoes (mostly monogenetic scoria cones and a few small shields) but also includes the polygenetic Tancítaro volcano, which all sum up to a total of ~326 ± 57 km^3 of emitted magma (Morelli et al., 2010). Apart from the well-studied Paricutin (e.g., Larrea et al., 2021 and references therein) and Tancítaro volcanoes (Di Traglia et al., 2014; Ownby et al., 2011), little is known of the other volcanoes in this region. Previous works reported whole-rock major-and-trace element analyses, isotopic ratios (Sr, Nd, Pb), and radiometric dates (^{40}Ar/^{39}Ar, K—Ar) for some of the volcanoes (e.g., Ban et al., 1992; Chesley et al., 2002; Hasenaka, 1992; Hasenaka and Carmichael, 1987; Johnson et al., 2009, 2010; Larrea et al., 2019a; Verma and Hasenaka, 2004), including a few samples from El Astillero and El Pedregal.

Larrea et al. (2019a) established the emplacement sequence of tephras and lava flows of both volcanoes, estimated the erupted volumes, and reported major element compositional ranges of their products. The eruption was characterized by a change from explosive to effusive activity, accompanied by a shift of the active vents which are located 3.5 km apart (Fig. 1). The eruption first formed El Astillero scoria cone and its associated tephra and lava field (EA LF1 to EA LF3) and continued with the emplacement of the El Pedregal lava flows (EP LF1 to EP LF5). The lava flows together occupy an area of 14.7 km^2 with an estimated volume of ~0.5 km^3 (dense rock equivalent). The composition of the emitted products progressively changed from basaltic andesite to andesite (SiO_2: 52–59 wt%), followed by a final reversal to more mafic compositions (Fig. 2). Their mineral assemblage comprises a variable amount of olivine, orthopyroxene, clinopyroxene, and plagioclase phenocrysts embedded in a holocrystalline to hypocrystalline groundmass (Larrea et al., 2019a). In accordance with the geochemical variation, the abundance of olivine decreased while that of pyroxene increased as the eruption progressed, with a final reversal to olivine-rich magmas. Based on the approach proposed by Pinkerton and Wilson (1994), effusion rates and viscosities that yielded lava flow advances of a few meters per day were calculated by Larrea et al. (2019a), who then estimated a total time for the emplacement of both volcanoes of ~6 years, assuming uninterrupted lava emission.

3. Material and methods

Fresh lava and tephra samples were collected spanning the entire eruptive sequence of El Astillero and El Pedregal volcanoes in space and time. These samples were studied macro- and microscopically, and 21 lavas and 8 tephra samples were selected for whole-rock analyses (see detailed sample preparation and analytical procedures in Appendix A). The lava sample selection covered all the eruptive stages from both eruptive centers (Fig. 1). The tephra selection includes three samples

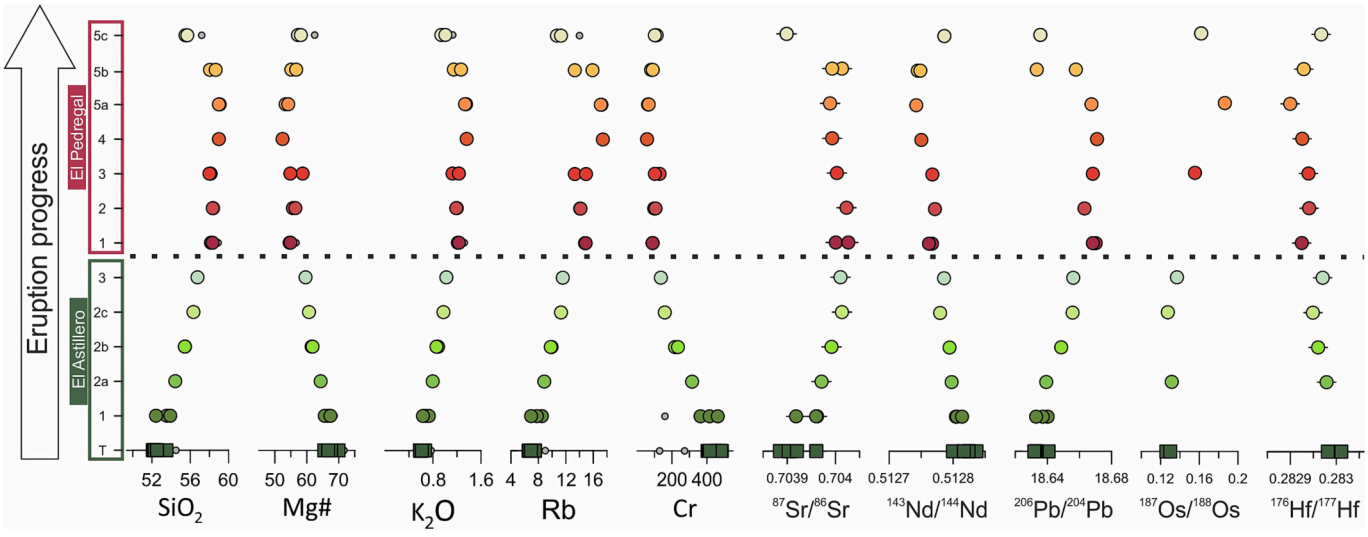

Fig. 2. Compositional variations of El Astillero and El Pedregal products (tephras and lavas) with time. Mg# = 100•Mg/(Mg + Fe^T) where Fe^T includes total iron as Fe^{2+}. Symbol designations and colors as in Fig. 1; small gray circles are El Astillero and El Pedregal data reported by Hasenaka (1992), Johnson et al. (2009), and Ownby et al. (2011). (For interpretation of the references to colour in this figure legend, the reader is referred to the web version of this article.)

directly collected in contact with the underlying paleosol (i.e., samples TANC-1806A, TANC-1828A, and TANC-1830A), which encompass the early explosive activity of El Astillero. Furthermore, two sites to the west of El Astillero cone were excavated and stratigraphically sampled to capture the full extent of Strombolian explosive activity in proximal areas (sites TANC-1808 and TANC-1826; Fig. 1); from these sites, four samples were selected spanning the vertical sequence.

The samples were analyzed at the Geoanalytical Laboratory at Washington State University by X-ray fluorescence spectrometry (XRF) for major and minor elements and inductively coupled plasma mass spectrometry (ICP-MS) for trace elements. Major element data from these samples were published in Larrea et al. (2019a). A subset of these samples, including 5 tephra and 16 lava samples, were analyzed for Sr, Nd, and Pb isotopes, and additionally, two tephra and twelve lava samples were prepared for Os and Hf isotope measurements. Sample preparation for Sr, Nd, Pb, Hf, and Os isotopes were performed at Miami University (Ohio, USA); Sr, Nd, and Os were measured by a Thermo-Finnigan Triton thermal ionization mass spectrometer (TIMS), whereas Pb and Hf were measured by a Nu Instruments Plasma 3D multi-collector ICP-MS. El Astillero and El Pedregal whole-rock geochemical

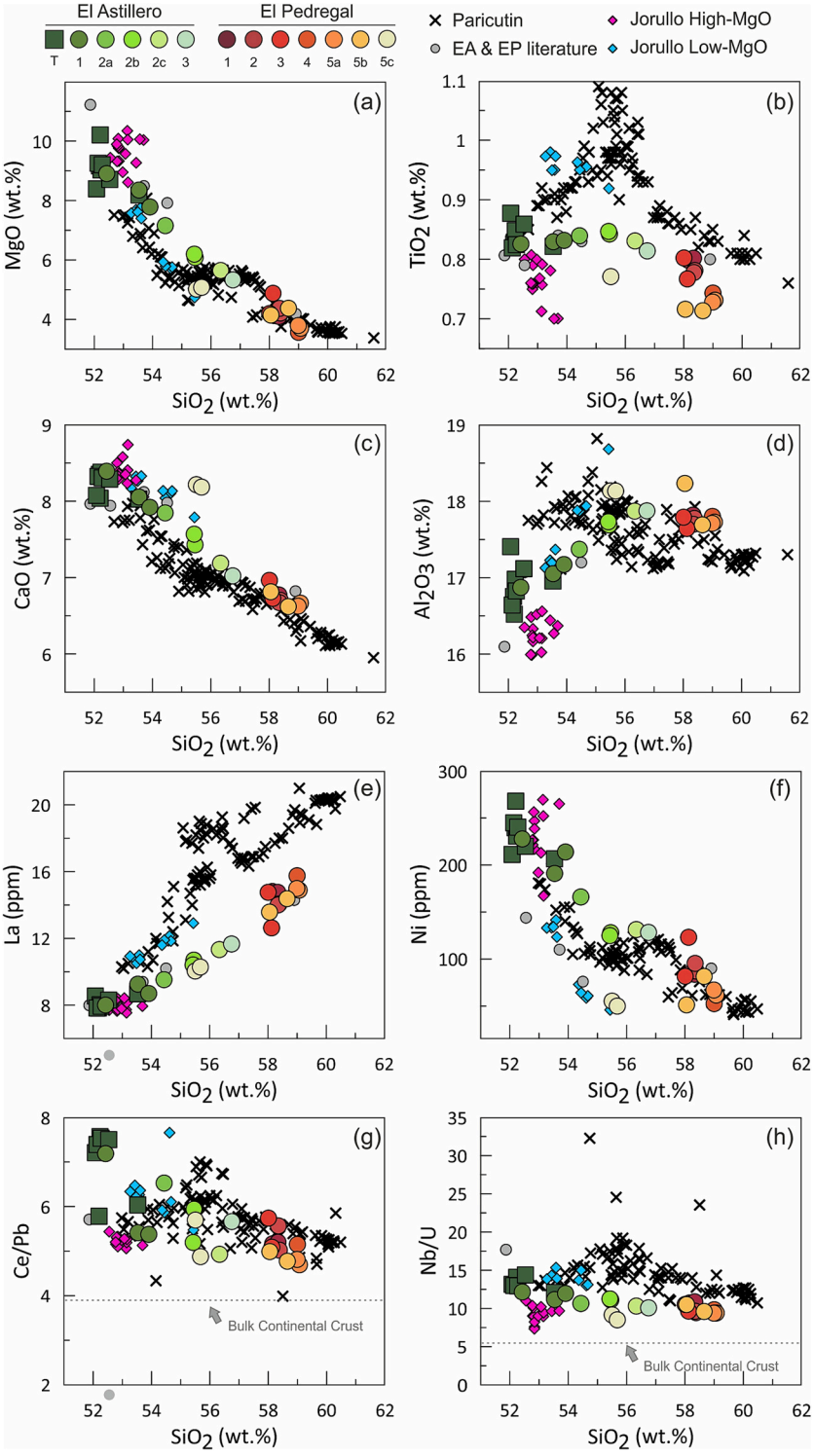

Fig. 3. Selected whole-rock major and trace element abundances, and trace element ratios vs. SiO_2 (wt%) for El Astillero (EA) and El Pedregal (EP) tephras and lavas analyzed in this study. Symbol designations and colors as in Fig. 1; small gray circles are EA and EP data reported by Hasenaka (1992), Johnson et al. (2009), and Ownby et al. (2011). Data for Jorullo (diamonds) and Paricutin (crosses) historic eruptions are from Rasoazanamparany et al. (2016) and Larrea et al. (2017, 2019b), respectively. Bulk continental crust trace element ratios (from Rudnick and Gao, 2003; not correlated with SiO_2 wt %) are shown in panels g) and h) as a dashed line. (For interpretation of the references to colour in this figure legend, the reader is referred to the web version of this article.)

results are listed in Appendix B - Table B.1.

4. Results

4.1. Whole-rock chemistry

4.1.1. Major and trace elements

The composition of sampled tephra deposits and lava flows ranges from basaltic andesite to andesite (Larrea et al., 2019a) following the total alkalis vs. silica (TAS) classification by Le Bas et al. (1986); all the volcanic products erupted from El Astillero classify as basaltic andesites, while El Pedregal lavas are mostly andesites, except for the last lava flow emplaced (LF-5c), which classifies as a basaltic andesite (Fig. 6 in Larrea et al., 2019a). In accordance, as previously described by Larrea et al. (2019a), the volcanic products show a progressive evolution in composition throughout the eruptive sequence for most major and trace elements, although a compositional shift to a more primitive composition at the end of the eruption is particularly notable in LF-5b (i.e., K_2O and Rb, see Fig. 2) and in LF-5c (i.e., SiO_2, #Mg and Cr, see Fig. 2). Moreover, minor reversals in Mg# are observable in the lava sequence of El Pedregal (LF-1 to LF-5; Fig. 2).

Bivariate plots of selected major elements versus SiO_2 (wt%) are presented in Fig. 3a-d. Most volcanic products from El Astillero and El Pedregal (EA-tephra to EP–LF5a; Fig. 3) display a continuous liquid line of descent, apart from the last lava flows (LF-5b and LF-5c) emitted from El Pedregal. MgO, CaO, and FeO^T decrease with increasing SiO_2, Al_2O_3, Na_2O, K_2O, while P_2O_5 increases with increasing SiO_2, and TiO_2 shows variable behavior with a kink at 55.5 wt% SiO_2. Whole-rock trace element abundances also correlate with SiO_2 (see selected trace elements in Fig. 3e-f). Incompatible elements such as La and Ba show positive correlations with increasing SiO_2, whereas compatible trace elements such as Ni, Cr, and Sc show negative correlations with increasing SiO_2. As observed for major elements, there is also a shift to a more primitive composition at the end of the eruption (see LF-5b and LF-5c in Fig. 2 and Fig. 3e-f). Remarkably, the composition of LF-5b and LF-5c is unique and certain elements (e.g., MgO, TiO_2, CaO, Al_2O_3, and Ni) deviate strongly from the main compositional trends of the eruptive sequence.

All tephra and lava samples from El Astillero and El Pedregal have lower Ce/Pb and Nb/U relative to MORB and OIB (Ce/Pb > 25; Nb/U > 47; e.g., Hofmann (1988), Sun and McDonough (1989), and Workman and Hart (2005)), but show a slight decrease in Ce/Pb and Nb/U with increasing SiO_2, pointing towards bulk continental crust compositions (Rudnick and Gao, 2003; Fig. 3g-h).

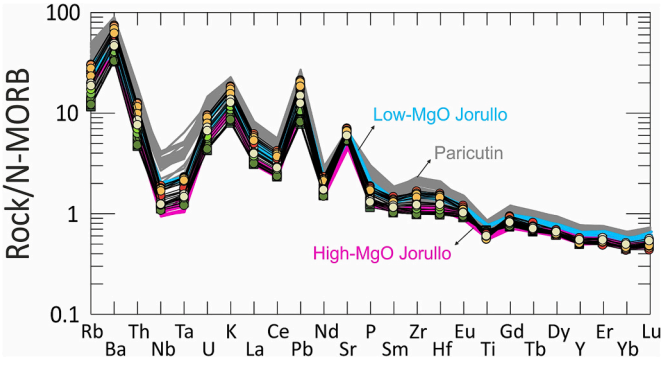

Fig. 4. N-MORB-normalized (Sun and McDonough, 1989) multi-element diagrams for El Astillero and El Pedregal tephras and lavas. Symbol designations and colors as in Fig. 1. Data from Jorullo (blue and pink polygons) and Paricutin (gray polygon) eruptions are from Rasoazanamparany et al. (2016), and Larrea et al. (2017, 2019b), respectively. (For interpretation of the references to colour in this figure legend, the reader is referred to the web version of this article.)

In the N-MORB-normalized multi-element diagram (Sun and McDonough, 1989; Fig. 4), El Astillero and El Pedregal volcanic products show typical arc trace-element patterns with enrichments in fluid-mobile large-ion lithophile elements (LILE) such as Rb, Ba, K, Pb, and Sr, and depletions in high-field strength elements (HFSE) such as Nb and Ta. In addition, the patterns exhibit an enrichment in light rare earth elements (LREE) and a depletion in heavy rare earth elements (HREE) relative to normal mid-oceanic basalts (N-MORB).

4.1.2. Isotopic data

The Sr-Nd-Pb-Hf-Os isotope data obtained for the studied tephras and lavas are plotted in Figs. 2 and 5. The $^{87}Sr/^{86}Sr$ isotopic ratios range from 0.70388 to 0.70403, $^{143}Nd/^{144}Nd$ from 0.512836 to 0.512742, $^{206}Pb/^{204}Pb$ from 18.632 to 18.671, $^{207}Pb/^{204}Pb$ from 15.583 to 15.598, $^{208}Pb/^{204}Pb$ from 38.376 to 38.450, and $^{176}Hf/^{177}Hf$ from 0.28301 to 0.28290. The tephra and lava $^{187}Os/^{188}Os$ ratios range from 0.1258 to 0.1865 over a range in Os concentrations from 3 to 116 ppt. All samples, except El Astillero TANC-1830A (tephra) and TANC-1807 (lava), show more radiogenic $^{187}Os/^{188}Os$ ratios than primitive upper mantle values (~0.1296; Meisel et al., 1996). Overall, as the eruption progressed with time, lava and tephra samples from El Astillero display more radiogenic $^{87}Sr/^{86}Sr$, $^{206}Pb/^{204}Pb$, $^{207}Pb/^{204}Pb$, $^{208}Pb/^{204}Pb$, and $^{187}Os/^{188}Os$ and less radiogenic $^{143}Nd/^{144}Nd$ and $^{176}Hf/^{177}Hf$ ratios; however, the isotopic variation is smaller in El Pedregal lavas, and as identified for major and trace elements, there is a shift to distinct isotopic signatures in El Pedregal LF-5b and LF-5c samples, which deviate from the eruptive sequence trend for $^{87}Sr/^{86}Sr$ vs $^{143}Nd/^{144}Nd$ (Fig. 5).

5. Discussion

In the following sections the composition of the magmas erupted by El Astillero and El Pedregal volcanoes are compared to those from the Paricutin and Jorullo historic eruptions, with the aim to decipher their main sources of magma generation, and the mechanisms controlling subsequent geochemical evolution, including open-system processes.

5.1. Comparison to Jorullo and Paricutin: Eruption progression and magma evolution

The 1759 to 1774 eruption of Jorullo produced an alignment of five cones and issued a total bulk volume of ~2 km^3 of eruptive products, including pyroclastic deposits (0.36–0.5 km^3) and lava flows (0.54–1.5 km^3) forming a lava field of ~9 km^2 (Guilbaud et al., 2009; Luhr and Carmichael, 1985; Rowland et al., 2009). According to the historical records, the first years of the eruption (from 1759 to 1764) were characterized by frequent Strombolian activity that built the five cones along a fissure. This explosive activity continued intermittently almost until the end of the eruption, blanketing with tephra all but one of the lava flows, which were mostly emitted from 1760 to 1766 (Luhr and Carmichael, 1985); the volcano was reported inactive in 1774, but according to Gadow (1930) its activity may have ended earlier. Paricutin volcano, located 75 km to the NW of Jorullo (Fig. 1), erupted from February 20, 1943 until March 04, 1952 (Luhr and Simkin, 1993). During the first months of the eruption, violent Strombolian explosive activity (sensu Valentine and Connor, 2015) related to the vent opening stage quickly built a cone, followed by a steady-state effusive stage (Larrea et al., 2021). The first volume estimates suggested that during the nine-year period of eruption, ~1.38 km^3 of total bulk magma was emitted, including lavas and tephras (McBirney et al., 1987); however, more recently Larrea et al. (2017), with the aid of topographic reconstructions, calculated the lava field to be 25 km^2 constituted by 1.6 km^3 of dense rock equivalent. In comparison to these historic eruptions, the ~500–700 CE El Astillero and El Pedregal volcanoes were formed in a shorter time (<6 years), and emitted a lava field of ~14.7 km^2, an area intermediate in size between Jorullo (~9 km^2) and Paricutin (25 km^2). The estimated total lava volume of ~0.5 km^3 (DRE) for El Astillero and

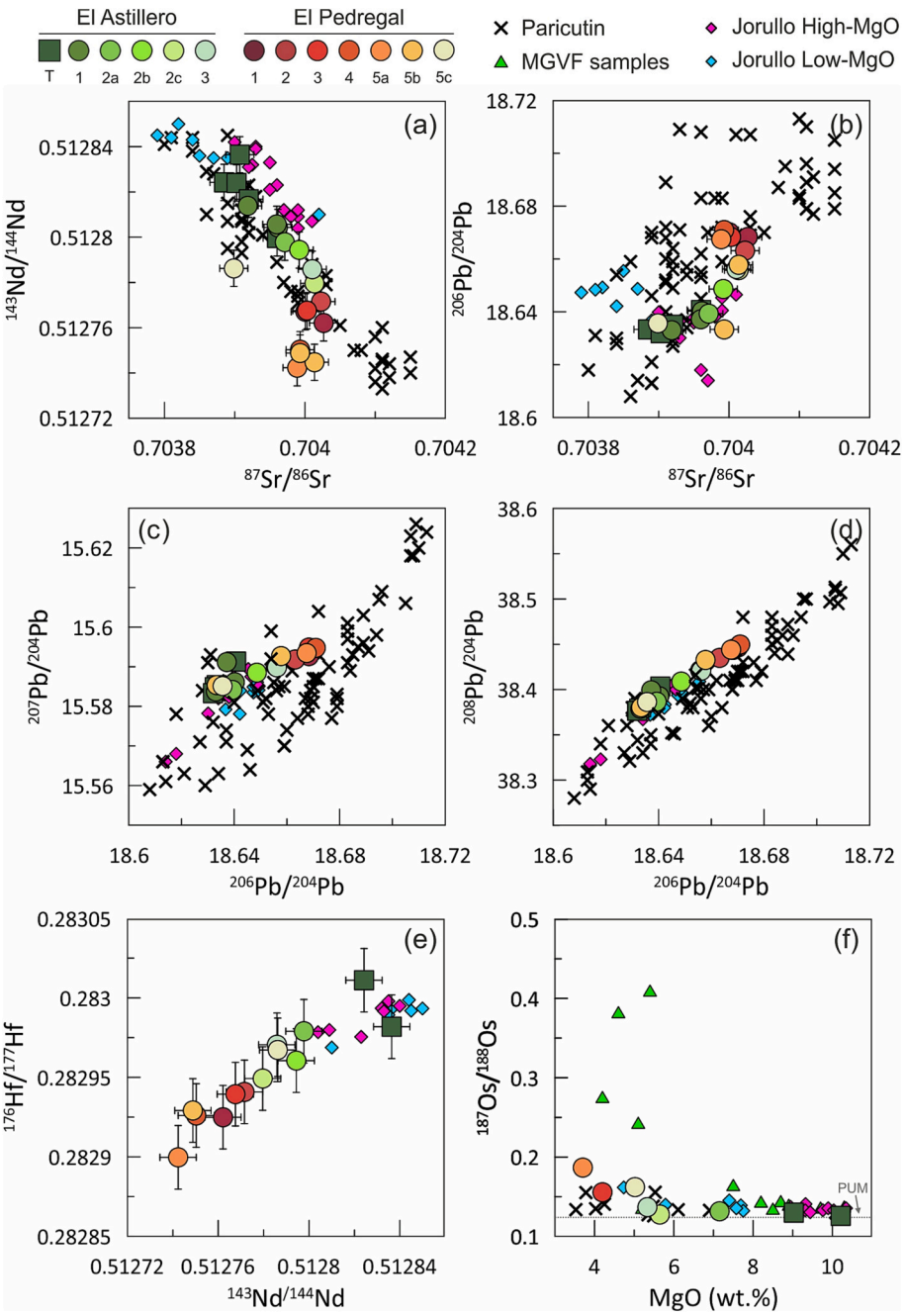

Fig. 5. Isotope variation diagrams for El Astillero and El Pedregal tephras and lavas. Isotope error bars when not indicated are smaller than the symbol size. Symbol designations and colors as in Fig. 1. Paricutin and Jorullo samples are shown for comparison. In panel f) Os data from the MGVF from Chesley et al. (2002) and the Primitive Upper Mantle (PUM) composition (not correlated with MgO wt% content) from Meisel et al. (2001) are also shown. (For interpretation of the references to colour in this figure legend, the reader is referred to the web version of this article.)

El Pedregal is similar to Jorullo's minimum volume estimate, but much smaller than Paricutin's. Regarding the eruptive style, El Astillero and El Pedregal followed a similar pattern to that of Jorullo and Paricutin, with intense initial explosive activity that then turned mostly effusive; however, Jorullo returned several times briefly to an explosive style as the eruption progressed, while El Pedregal was entirely effusive.

Jorullo and Paricutin products gradually became more differentiated in composition with time (Larrea et al., 2019b; Rasoazanamparany et al., 2016), ranging from basalts to basaltic andesites in Jorullo, and from basaltic andesites to andesites in Paricutin (Luhr and Carmichael, 1985; Wilcox, 1954). This trend is also observable at El Astillero and El Pedregal, where the volcanic products range in composition from basaltic andesites to andesites, but followed by a final reversal to more mafic compositions (i.e., basaltic andesites from El Pedregal LF-5b and LF-5c; Fig. 2). For most major and trace elements El Astillero tephras show a compositional range similar to Jorullo's high-MgO products (Fig. 3; Larrea et al., 2019b; Rasoazanamparany et al., 2016), and the lava flows from El Astillero and El Pedregal show a compositional range broadly similar to that of Jorullo's low-MgO and Paricutin's products taken together, although they show distinct lower/higher contents in certain elements (e.g., TiO_2 and La; Fig. 3) and do not reach a SiO_2 content quite as high as that of Paricutin volcano. The N-MORB-normalized (Sun and McDonough, 1989) multi-element patterns of El Astillero and El Pedregal are also similar to those of Paricutin and Jorullo volcanoes (Fig. 4; Larrea et al., 2019b; Rasoazanamparany et al., 2016), and the isotopic compositions display coinciding trends (Fig. 5; Larrea et al., 2019b; Rasoazanamparany et al., 2016), although Paricutin magmas show a broader isotopic variation.

Despite these geochemical similarities, products of the Jorullo and Paricutin historic eruptions were previously considered to represent opposite endmembers in a petrogenetic model that postulated that their compositional variations resulted from different degrees of crustal

contamination. Accordingly, Paricutin magmas show significant contamination while Jorullo's magmas had traversed the crust with limited crustal interaction (e.g., Cebriá et al., 2011; Erlund et al., 2010; Luhr, 2001; McBirney et al., 1987; Rowe et al., 2011; Wilcox, 1954). Recent studies have re-evaluated the chemical signatures of both volcanoes and their compositional variations were alternatively explained by a combination of variable degrees of mafic magma recharge, magma mixing, and fractional crystallization of magmas derived from a heterogeneous subduction-modified mantle (Rasoazanamparany et al., 2016 and Larrea et al., 2019b, 2021, respectively). In these new models, crustal assimilation is insignificant.

The continuous compositional trend in major and trace elements defined by the El Astillero tephras to El Pedregal LF-5a lava sequence is compatible with fractional crystallization. The marked decreases in MgO, FeO^T, CaO, Ni, and Cr with increasing SiO_2, together with the increase in Na_2O, K_2O, P_2O_5, and La with increasing SiO_2 (Fig. 3), are consistent with progressive fractionation of olivine, orthopyroxene, and clinopyroxene. In addition, the change from increasing to decreasing TiO_2 at $SiO_2 \sim 55.5$ wt% indicates that Fe—Ti oxides join the fractionating mineral assemblage at that point. The slight increase in Al_2O_3 (Fig. 3) and Sr with increasing SiO_2 together with the lack of negative Eu anomalies (Fig. 4) suggest that plagioclase was not an important fractionating mineral phase. This proposed fractionating mineral assemblage is in accordance with the petrographic descriptions carried out by Larrea et al. (2019a). The increase in highly incompatible element abundances such as Rb, Ba, Nb, La, and Zr with increasing SiO_2 (Figs. 2 and 3) is also consistent with fractional crystallization. However, the composition of some samples from El Astillero and El Pedregal point

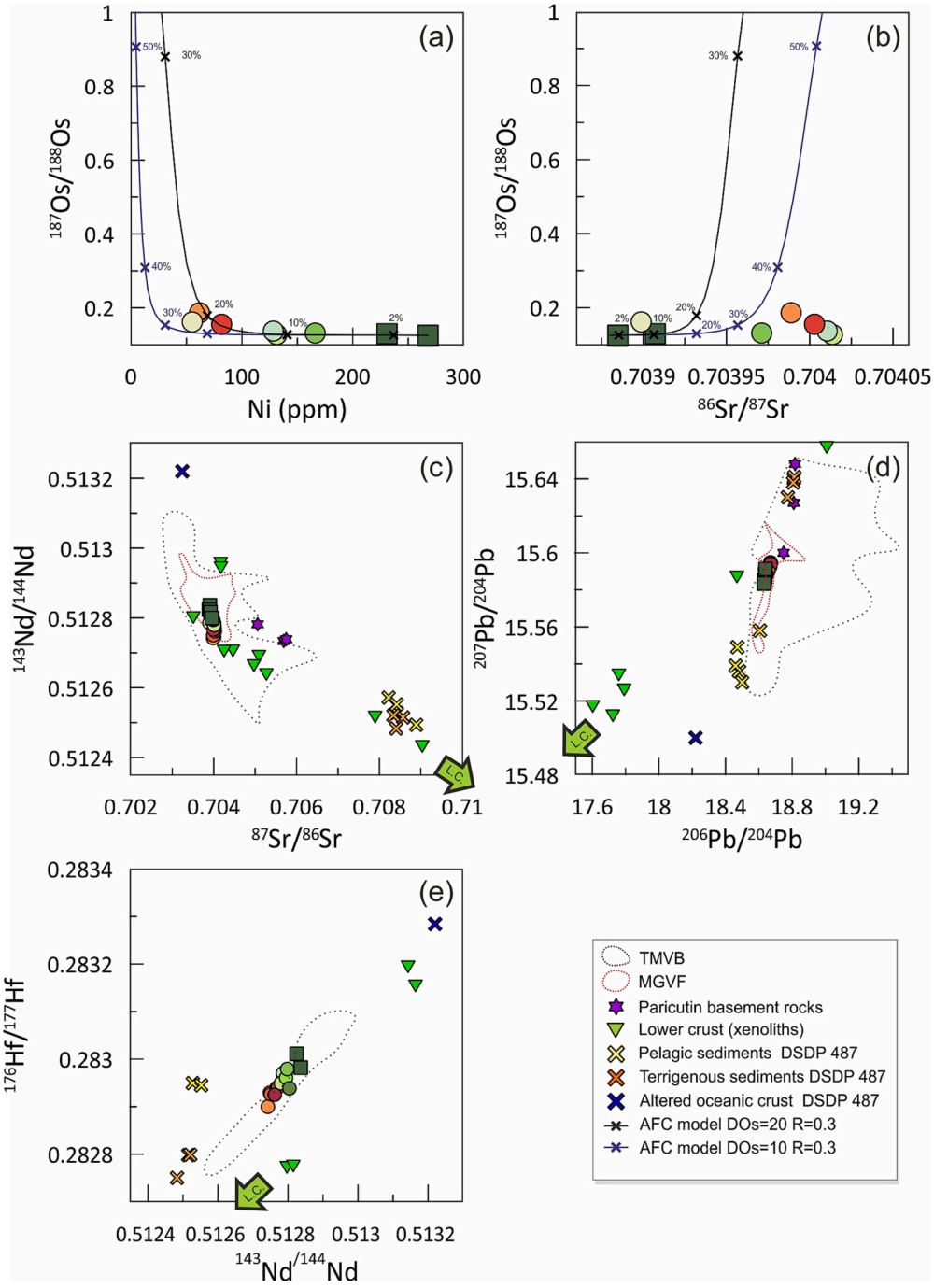

Fig. 6. Plots **(a)** $^{187}Os/^{188}Os$ vs Ni and **(b)** $^{187}Os/^{188}Os$ vs $^{87}Sr/^{86}Sr$ for El Astillero and El Pedregal samples with assimilation-fractional crystallization (AFC) models of upper crust represented by the mean composition of Paricutin basement rocks. AFC curves were calculated using bulk DOs of 10 and 20 with a fixed $R = 0.3$ (see text for further explanation, and Appendix B - Table B.2 for modelling parameters). **(c-e)** Sr, Nd, Pb, and Hf isotopic variations of El Astillero and El Pedregal tephra and lava samples (symbol designations and colors as in Fig. 1) plotted together with TMVB data from Gómez-Tuena et al. (2007a, 2007b), Luhr et al. (2006), Cai et al. (2014), and MGVF data from Blatter and Hammersley (2010), the slab components (terrigenous sediments, pelagic sediments and the average altered oceanic crust from DSDP site 487; LaGatta, 2003; Verma, 2000), and potential contaminants, including Paricutin basement granitoids (Larrea et al., 2019b) and lower crust xenoliths (Lawlor et al., 1999; Schaaf et al., 1994; Vervoort et al., 2000). Green arrow shows the geochemical trend described by the lower crust xenoliths (L.C.). (For interpretation of the references to colour in this figure legend, the reader is referred to the web version of this article.)

towards open-system processes such as magma recharge (see discussion section 5.4 below). Additionally, the occurrence of a quartz xenocryst in sample TANC-1815 (EP- LF3) surrounded by a reaction rim of pyroxenes (Larrea et al., 2019a) suggests minor crustal contamination, although the whole-rock composition of this sample does not differ from others among the studied rocks.

In the following sections, we evaluate the potential contributions of crustal assimilation and mantle source heterogeneity in the genesis of El Astillero and El Pedregal magmas.

5.2. The role of crustal assimilation

The effect of crustal contamination can be evaluated by the relationship of highly incompatible trace element ratios against indices of differentiation (e.g., SiO_2) and isotopic signatures, as assimilation will imprint enriched signatures on the magmas. El Astillero and El Pedregal magmas show low Ce/Pb and Nb/U ratios close to the bulk continental crust (Fig. 3g-h), a negative correlation of $^{87}Sr/^{86}Sr$ vs. $^{143}Nd/^{144}Nd$ (Fig. 5a), supra-chondritic $^{187}Os/^{188}Os$ (Fig. 5f), and a slight correlation of Sr-Nd-Pb-Os-Hf isotope ratios with SiO_2. This progressive change is observable from the initiation of the eruption to El Pedregal LF-5a lava and could be explained by AFC (assimilation + fractional crystallization). However, the occurrence of the compositional reversal at the end of the eruption, affecting El Pedregal LF-5b and LF-5c lavas (observable in petrography, major and trace elements, and isotopes), is opposite to the pattern typically expected for AFC processes.

We conducted AFC modelling to check the potential influence of crustal contamination, and to further evaluate if the radiogenic Os isotopic signatures observed in some samples from El Astillero and El Pedregal reflect crustal assimilation by subduction related magmas. The tephra TANC-1830A was selected as a starting point because it is closest in composition to a primary magma (see modelling parameters in Appendix B - Table B.2). The mean basement composition from Larrea et al. (2019b) was used to represent the potentially assimilated material, because the tephra and lava samples from El Astillero and El Pedregal exhibit Sr-Nd-Pb isotopic trends that extend towards the composition of the local granitic basement, but opposite to that of the Mexican lower crustal xenoliths (Fig. 6c-e). The AFC trends were calculated assuming bulk distribution coefficients of $D_{Os} = 10$ and 20 and reasonable rates of assimilation to fractional crystallization (i.e., $R < 1$). As observed in Fig. 6d, the Ni contents and low $^{187}Os/^{188}Os$ ratios displayed by El Astillero and El Pedregal samples could be reproduced with <20–25% AFC and $R = 0.3$, implying that the Os isotopic signatures could be influenced by variable degrees of AFC. Nonetheless, the lack of correlation between Os and Sr–Nd–Pb isotopes (e.g., Fig. 6b), and the absence of petrographic evidence for crustal assimilation argue against AFC as the main process responsible for the Sr–Nd–Pb-Hf isotopic variations in the samples. The Os isotopes are more prone to be affected by assimilation than the Sr-Nd-Pb isotopes, due to the low Os contents in El Astillero and El Pedregal samples (<120 ppt), a feature also observed in the Tacámbaro monogenetic cluster (Guilbaud et al., 2019). Similarly, Paricutin and Jorullo samples have relatively low and constant $^{187}Os/^{188}Os$ ratios compared to other MGVF magmas (Fig. 5f), which has been interpreted to be inconsistent with significant crustal assimilation (Larrea et al., 2019b; Rasoazanamparany et al., 2016).

5.3. Mantle source heterogeneity

Several studies of TMVB arc magmas have concluded that near-primary melts that originate in the subduction-modified mantle wedge pass through the crust almost unaffected (e.g., Gómez-Tuena et al., 2007a, 2008, 2018; Guilbaud et al., 2019; Larrea et al., 2019b; Rasoazanamparany et al., 2016; Siebe et al., 2004; Straub et al., 2008, 2013). As discussed above, given the limited role of crustal assimilation in controlling the Sr-Nd-Pb-Hf isotope ratios of El Astillero and El Pedregal magmas, mantle source heterogeneity is considered to better explain their chemical characteristics; this heterogeneity could result from compositional differences in the fluids or mantle domains that contributed to the melts, or in differing proportions of slab fluids involved in the partial melting of the mantle source materials.

The Sr-Nd-Pb-Hf isotopic compositions of El Astillero and El Pedregal magmas fall within the range of the TMVB (Cai et al., 2014; Gómez-Tuena et al., 2007a, 2007b; Luhr et al., 2006) and the MGVF products (Blatter and Hammersley, 2010), and are well bracketed by the slab components including the altered oceanic crust (AOC) and the trench sediments (Fig. 6c-e). Similar to Paricutin and Jorullo, El Astillero and El Pedregal samples show strong correlations in $^{87}Sr/^{86}Sr$ vs.$^{143}Nd/^{144}Nd$, $^{207}Pb/^{204}Pb$ and $^{208}Pb/^{204}Pb$ vs. $^{206}Pb/^{204}Pb$, and $^{143}Nd/^{144}Nd$ vs. $^{176}Hf/^{177}Hf$ (Fig. 5a-e), indicating that at least two components were involved in their petrogenesis. In addition, the LILE enrichments and HFSE depletions in the samples (Fig. 4) strongly suggest the involvement of subduction-related hydrous fluids in their petrogenesis, and the low Ce/Pb and Nb/U ratios (Fig. 3g-h) seem to reflect crustal recycling into the mantle. Consequently, we investigate the possibility that El Astillero and El Pedregal magmas could originate by addition of subduction components (AOC + trench sediments) to a pre-subduction mantle wedge.

We modeled El Astillero and El Pedregal trace element and isotope data using the composition of the Mexican pre-subduction mantle wedge, and the Cocos Plate products being subducted beneath the TMVB sampled at the DSDP site 487 (e.g., Cai et al., 2014; Gómez-Tuena et al., 2003, 2007a, 2007b; Verma, 2000). The mantle wedge was interpreted to be similar to the Northern Mexican Extensional Province mantle source (Luhr et al., 2006; Fig. 7) with a depleted mantle (DMM) trace element composition (Salters and Stracke, 2004), and the Sr-Nd-Pb-Hf isotopic composition of magma with the least slab signature in central Mexico (the Old Texcal Flow from Straub et al., 2015). The trace element and isotopic composition of the subducted AOC was recalculated by Straub et al. (2015) according to its inferred age of ~5–6 million years, and the pelagic and terrigenous sediments were analyzed for trace element abundances and Sr-Nd-Pb-Hf isotopes by LaGatta (2003) and Cai et al. (2014). The trace element composition of the subducting Cocos plate-derived fluid was calculated by using the mobility data of Kessel et al. (2005) at 900–800 °C and 4 GPa, and for sediment-derived fluid the D values at 700 °C from Johnson and Plank (1999) were used. The total extraction of hydrous fluid during dehydration was assumed to be 1.5 wt% in both oceanic crust and sediment. All parameters used in the model in Fig. 7a–c are given in Appendix B – Table B.3.

El Astillero and El Pedregal samples have higher $^{87}Sr/^{86}Sr$ and lower $^{143}Nd/^{144}Nd$ ratios than most of the NMEP samples (Luhr et al., 2006; Fig. 7a), consistent with derivation from a subduction-enriched mantle wedge. In order to reproduce the $^{87}Sr/^{86}Sr$ vs. $^{206}Pb/^{204}Pb$ isotopic trend (Fig. 7b) the existence of two subduction components is required, as previously proposed for Paricutin and Jorullo magmas (Fig. 7; Larrea et al., 2019b; Rasoazanamparany et al., 2016). The isotopic mixing models presented in Fig. 7a-c show that in order to reproduce the trend of the El Astillero and El Pedregal products in Sr-Nd-Pb-Hf isotope space, mixing between the mantle wedge and a slab component (SC1) composed of ~70% sediment-derived fluid (70:30 terrigenous to pelagic) and ~ 30% AOC-derived fluid is needed to produce a metasomatized mantle (~2% subduction component) that is subsequently metasomatized again (<8%, including Paricutin and Jorullo magmas; zoomed-in inset in Fig. 7a-c) by a second slab component (SC2) consisting of ~90% sediment-derived fluid (99:1 terrigenous to pelagic) and ~ 10% AOC-derived fluid. The observed differences in the proportions of sediment types (SC1 versus SC2) may be attributed to either the heterogeneity of the sediment pile itself and/or the incomplete homogenization of a heterogeneous sediment-derived fluid, as highlighted by Rasoazanamparany et al. (2016) in the case of Jorullo volcano. Alternatively, as proposed by Patino et al. (2000), these variations could be linked to the presence of horst and graben structures within the subducting plate. Such structural features may result in variable

sediment proportions, with a higher abundance of terrigenous sediment in the graben structure due to scraping off from the adjacent horst.

This mixing scenario, based on Sr-Nd-Pb-Hf isotope systematics and involving the Mexican pre-subduction depleted mantle wedge and the described subduction components SC1 and SC2, was also used for trace element modelling (Fig. 8). The depleted mantle was assumed to have a typical upper mantle mineralogy of 55% olivine, 32% orthopyroxene, 10% clinopyroxene, and 3% garnet (e.g., Carter, 1970), and the mineral-melt partition coefficients were taken from Salters and Stracke (2004) and Stracke and Bourdon (2009); see Appendix B –Table B.4 for all

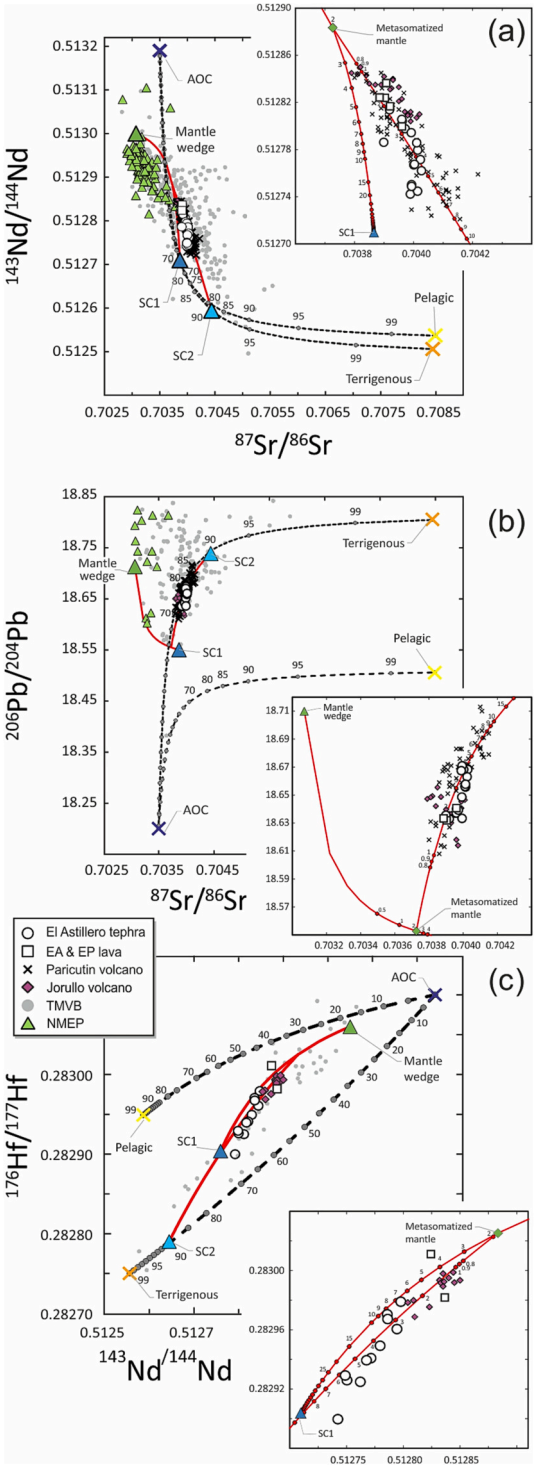

(caption on next column)

Fig. 7. Isotopic modelling of El Astillero and El Pedregal (EA & EP) tephras and lavas: **a)** $^{87}Sr/^{86}Sr$ vs. $^{143}Nd/^{144}Nd$, **b)** $^{87}Sr/^{86}Sr$ vs. $^{206}Pb/^{204}Pb$, and **c)** $^{143}Nd/^{144}Nd$ vs. $^{176}Hf/^{177}Hf$ showing mixing between the mantle wedge and potential subduction components with variable mixtures of altered oceanic crust (AOC) and pelagic and terrigenous sediment derived fluids. The black dashed curves indicate mixing between sediment-derived fluid (with 100% of terrigenous and 100% pelagic sediment) and AOC-derived fluids. The red solid curves represent the mixing between the mantle wedge and two calculated slab components SC1 and SC2 (blue triangles; zoomed in within the insets). Tick marks (gray and red dots throughout the curves) show the relative proportions of these mixing components. The studied samples are reproduced by a mixing model of the mantle wedge plus 2% subduction fluid SC1 derived from 70% sediment (70:30 terrigenous:pelagic) and 30% AOC, and a subsequent addition of up to 8% of subduction fluid SC2 derived from 90% sediment (99:1 terrigenous:pelagic) and 10% AOC. Mafic alkaline Northern Mexican Extensional Province (NMEP) type mantle data from Luhr et al. (2006) and TMVB data from Gómez-Tuena et al. (2007a, 2007b), Luhr et al. (2006), and Cai et al. (2014) are also plotted. See text for detailed explanation of the isotopic model, and Appendix B – Table B.3 for all the used model parameters. (For interpretation of the references to colour in this figure legend, the reader is referred to the web version of this article.)

model parameters. The presence of garnet in the source region is indicated by the high Dy/Yb (1.9 to 2.2) values of El Astillero and El Pedregal samples in comparison to N-MORB (Dy/Yb ~1.5). The trace element abundances of the most primitive magmas (i.e., El Astillero tephras) can be generated by ~10% batch melting of the SC1 + SC2-metasomatised mantle (Fig. 8). However, this model predicts higher concentrations for some of the highly fluid-mobile elements such as Cs, Rb, Ba, and Pb, which could be attributed to their significant loss during dewatering in the forearc (e.g., Schmidt and Poli, 1998) as previously inferred in other studies of the TMVB (e.g., Gómez-Tuena et al., 2007a; Guilbaud et al., 2019; Johnson et al., 2009; Rasoazanamparany et al., 2016). It is important to note that slight variations in the compositions and/or relative contributions of the subduction components (AOC + sediments) to the Mexican pre-subduction mantle, the percentage of fluid added, and/or the degree of partial melting could also explain the existing isotopic variability in Sr-Nd-Pb-Hf-Os of most of the mafic TMVB magmas, including the ones from El Astillero and El Pedregal (Fig. 7; Appendix B – Table B.3).

5.4. *Evidence for mafic magma recharge*

As discussed in the previous sections, our results show that El Astillero and El Pedregal melts were extracted from a subduction-modified mantle, without significant influence from crustal assimilation; in contrast, fractional crystallization is the main magmatic process governing the differentiation of these magmas through time. This combination of processes is reflected in the petrographic and geochemical progression of the El Astillero and El Pedregal products throughout their stratigraphic sequence (i.e., the evolutionary path observed in major elements, trace elements, and isotope ratios; Figs. 2-4) from the initiation of the eruption until the emission of El Pedregal LF-5a. Nevertheless, the occurrence of slight reversals in Mg# within the lava sequence of El Pedregal (LF-1 to LF-5; Fig. 2) is likely indicative of small mafic recharge events by one or more similar parental magmas, although the relative volume of these recharge events has not been quantified. A similar scenario was described for the eruptive sequence of Paricutin volcano where the identified Mg# reversals were successfully modeled using the Magma Chamber Simulator (Bohrson et al., 2014; https://mcs.geol.ucsb.edu/) considering open-system magma evolution with primitive magma replenishments during cooling and crystallization (Larrea et al., 2019b, 2021).

In addition, the final shift in composition observed towards the end of the El Pedregal eruption (i.e., LF-5b and 5c; Figs. 2-4) indicates the introduction of a new and distinct magma batch. These lava flows, 5b and 5c, exhibit compositions that deviate from the previous geochemical

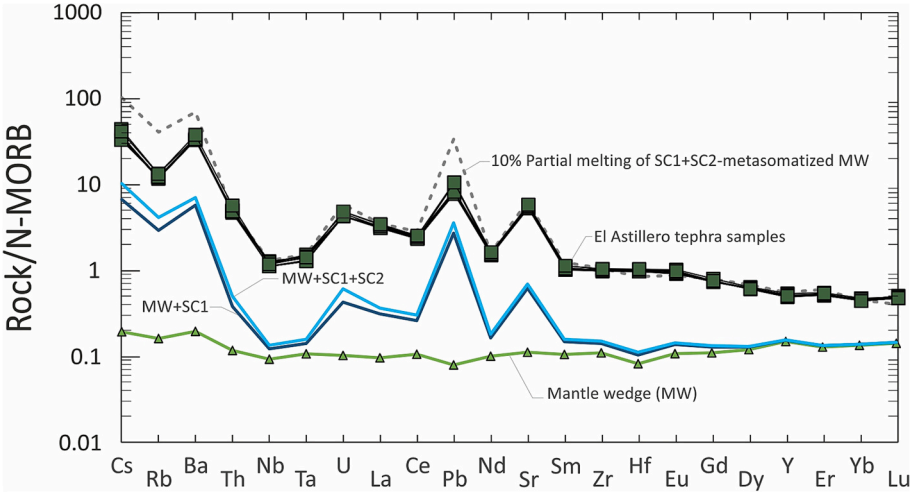

Fig. 8. Trace element modelling results showing the calculated mantle source composition for the mantle wedge (MW) plus 2% subduction fluid SC1 (dark blue line), and addition of 8% of subduction fluid SC2 (light blue line), using the mixture described in Fig. 7, and the magma derived by batch melting of the SC1 + SC2-metasomatized mantle wedge. Note that the trace element pattern of El Astillero tephras, which are the most primitive samples from the cluster, can be closely reproduced by 10% batch melting of the metasomatized source. See text and Appendix B – Table B.3 and Table B.4 for all model parameters. (For interpretation of the references to colour in this figure legend, the reader is referred to the web version of this article.)

trend, as evidenced by variations in the abundances of several major and trace elements (e.g., MgO, TiO_2, CaO, Al_2O_3, and Ni vs. SiO_2; Fig. 3). Moreover, their $^{87}Sr/^{86}Sr$ vs. $^{143}Nd/^{144}Nd$ isotope ratios do not follow the main trend, but rather align with the array observed in the MGVF (see Fig. 6c). These abrupt compositional changes suggest that after the eruption of LF-5a the residual magma mixed with a new and distinct magma batch. This new magma batch was slightly different in composition from the initial El Astillero parental magma, and after mixing yielded unique compositions for LF-5b and LF-5c, which became progressively more primitive with time (Fig. 3).

Our model indicates that the chemical signatures and compositional variations of El Astillero and El Pedregal eruptive products can be explained by a combination of variable degrees of magma recharge, magma mixing, and fractional crystallization of mantle-derived signatures. This combination of processes involved in the genesis and evolution of the magmas has been proposed before for other monogenetic volcanoes in the MGVF and elsewhere, and is in agreement with previous works proposing that primitive magmas in the central part of the TMVB are melts from a subduction-modified mantle that pass through the crust without major interaction (Gómez-Tuena et al., 2007a, 2008, 2018; Larrea et al., 2019b; Rasoazanamparany et al., 2016; Siebe et al., 2004; Straub et al., 2008, 2013).

6. Conclusion

The multi-isotopic study presented in this work on El Astillero and El Pedregal magmas shows that these are subduction-modified mantle extracts. This implies a direct connection of these monogenetic volcanoes with their deep source, which is in accordance with the general models of Németh and Kereszturi (2015) for monogenetic volcanism. In addition, the relatively rapid ascent of these melts towards the surface minimizes the possible influence of crustal assimilation. Despite this, the magmatic processes that govern the evolution of these magmas are complex; we have identified within the El Pedregal eruptive sequence repeated recharge by similar small mafic batches of magma. Towards the end of the eruption, the arrival of a distinct magma batch (different from the prior recharge events) at El Pedregal produced two lava flows that differ significantly in composition from the previously established main geochemical trend. Thus, the magmatic evolution of the El Astillero and El Pedregal eruption was controlled by repeated magma recharge events, followed by cycles of mixing and crystal fractionation. Similar scenarios have been postulated not only for the two historic eruptions in the MGVF, Jorullo and Paricutin (Larrea et al., 2019b, 2021; Rasoazanamparany et al., 2016), but also for the young Tacámbaro cluster (Guilbaud et al., 2019). These comprehensive geochemical investigations of well-constrained monogenetic eruption sequences have presented compelling evidence that these seemingly straightforward small-scale volcanic systems, commonly known as monogenetic, exhibit a level of complexity that challenges the traditional perception. This finding has led to a paradigm shift in our understanding of the importance of open-system processes relative to closed-system processes during the course of monogenetic volcanic eruptions. It is therefore important to combine and contrast whole-rock studies with finer-scale analyses of mineral phases to further constrain open-system processes, as successfully demonstrated recently in the case of Paricutin volcano (Albert et al., 2020; Larrea et al., 2021). The combination of these geochemical tools to evaluate the origin and evolution of the magmas feeding short-lived eruptions in the MGVF is becoming more relevant since repeated seismic swarms have been registered during the last 25 years within a small region beneath the NE lower flank of Tancítaro stratovolcano (Legrand et al., 2023). These swarms may represent repeated attempts of magma trying to migrate towards the surface and hence, precursors to the birth of a new monogenetic volcano in this region.

Declaration of Competing Interest

The authors declare that they have no known competing financial interests or personal relationships that could have appeared to influence the work reported in this paper.

Acknowledgments

The authors are grateful to undergraduate and graduate students from Universidad de Chile: Daniela Parra, Miyali Riquelme, Lucas Sanhueza, and Valentina Villanueva, who helped in different stages of this project. The personnel of *Protección Civil* and Miguel Equihua (*Desarrollo Rural y Ecología*) of the municipality of Tancítaro are thanked for their help and assistance during fieldwork. This work was supported by the National Science Foundation (NSF) EAR 1853006 awarded to Dr. E. Widom and P. Larrea, and NSF MRI 1919658 awarded to E. Widom. Fieldwork campaigns by P. Larrea, S. Salinas, and C. Siebe were supported by *Dirección General de Asuntos del Personal Académico* through project UNAM-DGAPA IN-104221 granted to Claus Siebe. Patricia Larrea was supported by a UNAM-DGAPA postdoctoral fellowship (2018-2019), Proyecto de Instalación Académica - FCFM, Universidad de Chile (2019-2023), and Proyecto N°0285/2022 from Vicerrectoría de Investigación y Desarrollo (VID) - Universidad de Chile. Constructive reviews by K. Nemeth, an anonymous reviewer, and Editor G. Shellnutt are greatly acknowledged.

Appendix A. Supplementary data

Supplementary data to this article can be found online at https://doi.org/10.1016/j.lithos.2023.107302.

References

Albert, H., Larrea, P., Costa, F., Widom, E., Siebe, C., 2020. Crystals reveal magma convection and melt transport in dyke-fed eruptions. Sci. Rep. 10, 11632.

Ban, M., Hasenaka, T., Delgado-Granados, H., Takaoka, T., 1992. K–Ar ages of lavas from shield volcanoes in the Michoacan-Guanajuato volcanic field, Mexico. Geofis. Int. 31 (4).

Blatter, D.L., Hammersley, L., 2010. Impact of the Orozco Fracture Zone on the central Mexican Volcanic Belt. J. Volcanol. Geotherm. Res. 197, 67–84.

Bohrson, W.A., Spera, F.J., Ghiorso, M.S., Brown, G.A., Creamer, J.B., Mayfield, A., 2014. Thermodynamic model for energy-constrained open-system evolution of crustal magma bodies undergoing simultaneous recharge, assimilation and crystallization: the magma chamber simulator. J. Petrol. 55, 1685–1717.

Cai, Y., LaGatta, A., Goldstein, S.L., Langmuir, C.H., Gómez-Tuena, A., Pozzo, A.L.M., Carrasco-Nuñez, G., 2014. Hafnium isotope evidence for slab melt contributions in the Central Mexican Volcanic Belt and implications for slab melting in hot and cold slab arcs. Chem. Geol. 377, 45–55.

Carmichael, I.S., 2002. The andesite aqueduct: perspectives on the evolution of intermediate magmatism in west-central (105–99 W) Mexico. Contrib. Mineral. Petrol. 143 (6), 641–663.

Carter, J.L., 1970. Mineralogy and chemistry of the Earth's upper mantle based on the partial fusion-partial crystallization model. Geol. Soc. Am. Bull. 81, 2021–2034.

Cebriá, J.M., Martiny, B.M., López-Ruiz, J., Morán-Zenteno, 2011. The Parícutin calc-alkaline lavas: New geochemical and petrogenetic modelling constraints on the crustal assimilation process. J. Volcanol. Geotherm. Res. 201, 113–125.

Chesley, J., Ruiz, J., Righter, K., Ferrari, L., Gómez-Tuena, A., 2002. Source contamination versus assimilation: an example from the Trans-Mexican Volcanic Arc. Earth Planet. Sci. Lett. 195, 211–221.

Chevrel, M.O., Guilbaud, M.N., Siebe, C., 2016. The ~AD 1250 effusive eruption of El Metate shield volcano (Michoacán, Mexico): magma source, crustal storage, eruptive dynamics, and lava rheology. Bull. Volcanol. 78 (4), 1–28.

Di Traglia, F., Morelli, S., Casagli, N., Monroy, V.H.G., 2014. Semi-automatic delimitation of volcanic edifice boundaries: Validation and application to the cinder cones of the Tancitaro–Nueva Italia region (Michoacán–Guanajuato Volcanic Field, Mexico). Geomorphology 219, 152–160.

Erlund, E.J., Cashman, K.V., Wallace, P.J., Pioli, L., Rosi, M., Johnson, E., Delgado Granados, H., 2010. Compositional evolution of magma from Parícutin Volcano, Mexico: the tephra record. J. Volcanol. Geotherm. Res. 197, 167–187.

Gadow, H., 1930. Jorullo: The History of the Volcano Jorullo and the Reclamation of the Devastated District by Animals and Plants. Cambridge University Press, London, p. 101.

Gómez-Tuena, A., LaGatta, A., Langmuir, C., Goldstein, S., Ortega-Gutiérrez, F., Carrasco-Núñez, G., 2003. Temporal control of subduction magmatism in the Eastern Trans-Mexican Volcanic Belt: mantle sources, slab contributions and crustal contamination. Geochem. Geophys. Geosyst. 4, 9.

Gómez-Tuena, A., Langmuir, C.H., Goldstein, S.L., Straub, S.M., Ortega-Gutierrez, F., 2007a. Geochemical evidence for slab melting in the Trans-Mexican Volcanic Belt. J. Petrol. 48, 537–562.

Gómez-Tuena, A., Orozco-Esquivel, M.A., Ferrari, L., 2007b. Igneous petrogenesis of the Trans-Mexican Volcanic Belt. In: Alaniz-Alvarez, S.A., Nieto-Samaniego, A.F. (Eds.), Geology of Mexico: Celebrating the Centenary of the Geological Society of Mexico, Geological Society of America Special Paper, vol. 422, pp. 1–53.

Gómez-Tuena, A., Mori, L., Rincón-Herrera, N.E., Ortega-Gutiérrez, F., Solé, J., Iriondo, A., 2008. The origin of a primitive trondhjemite from the Trans-Mexican Volcanic Belt and its implications for the construction of a modern continental arc. Geology 36 (6), 471–474.

Gómez-Tuena, A., Cavazos-Tovar, J.G., Parolari, M., Straub, S.M., Espinaza-Pereña, R., 2018. Geochronological and geochemical evidence of continental crust 'relamination' in the origin of intermediate arc magmas. Lithos 322, 52–66.

Gómez-Vasconcelos, M.G., Macías, J.L., Avellán, D.R., Sosa-Ceballos, G., Garduño-Monroy, V.H., Cisneros-Máximo, G., Layer, P.W., Benowitz, J., López-Loera, H., Mendiola López, F., Perton, M., 2020. The control of preexisting faults on the distribution, morphology, and volume of monogenetic volcanism in the Michoacán-Guanajuato volcanic field. Geol. Soc. Am. Bull. 132 (11–12), 2455–2474.

Guilbaud, M.N., Siebe, C., Salinas, S., 2009. Excursions to Paricutin and Jorullo (Michoacán), the youngest volcanoes of the Trans-Mexican Volcanic Belt. In: A Commemorative Fieldtrip on the Occasion of the 250th anniversary of Volcán Jorullo's Birth on September 29, 1759. Impretei, Mexico DF (31 pp.).

Guilbaud, M.N., Siebe, C., Layer, P., Salinas, S., Castro-Govea, R., Garduño-Monroy, V.H., Le Corvec, N., 2011. Geology, geochronology, and tectonic setting of the Jorullo Volcano region, Michoacán, México. J. Volcanol. Geotherm. Res. 201 (1–4), 97–112.

Guilbaud, M.N., Siebe, C., Layer, P., Salinas, S., 2012. Reconstruction of the volcanic history of the Tacámbaro-Puruarán area (Michoacán, México) reveals high frequency of Holocene monogenetic eruptions. Bull. Volcanol. 74 (5), 1187–1211.

Guilbaud, M.N., Siebe, C., Rasoazanamparany, C., Widom, E., Salinas, S., Castro Govea, R., 2019. Petrographic, geochemical and isotopic (Sr–Nd–Pb–Os) study of Plio-Quaternary volcanics and the Tertiary basement in the Jorullo-Tacámbaro area, Michoacán-Guanajuato volcanic field, Mexico. J. Petrol. 60 (12), 2317–2338.

Hasenaka, T., 1992. Contrasting volcanism in the Michoacán-Guanajuato volcanic field, Central Mexico: Shield volcanoes vs. cinder cones. In: Aoki, K. (Ed.), Subduction Volcanism and Tectonics of Western Mexican Volcanic Belt: Sendai. Tohoku University, Japan, p. 248.

Hasenaka, T., Carmichael, I.S.E., 1985a. A compilation of location, size, and geomorphological parameters of volcanoes of the Michoacan-Guanajuato volcanic field, Central Mexico. Geofis. Int. 24 (4), 577–607.

Hasenaka, T., Carmichael, I.S.E., 1985b. The cinder cones of Michoacán-Guanajuato, Central Mexico: their age, volume and distribution, and magma discharge rate. J. Volcanol. Geotherm. Res. 25, 105–124.

Hasenaka, T., Carmichael, I.S.E., 1987. The cinder cones of Michoacán-Guanajuato, Central Mexico: petrology and chemistry. J. Petrol. 28, 241–269.

Hofmann, A.W., 1988. Chemical differentiation of the Earth: the relationship between mantle, continental crust, and oceanic crust. Earth Planet. Sci. Lett. 90, 297–314.

Johnson, M.C., Plank, T., 1999. Dehydration and melting experiments constrain the fate of subducted sediments. Geochem. Geophys. Geosyst. 1, 1999GC000014.

Johnson, E.R., Wallace, P.J., Delgado Granados, H., Manea, V.C., Kent, A.J., Bindeman, I. N., Donegan, C.S., 2009. Subduction-related volatile recycling and magma generation beneath Central Mexico: insights from melt inclusions, oxygen isotopes and geodynamic models. J. Petrol. 50 (9), 1729–1764.

Johnson, E.R., Wallace, P.J., Cashman, K.V., Granados, H.D., 2010. Degassing of volatiles (H2O, CO2, S, Cl) during ascent, crystallization, and eruption at mafic monogenetic volcanoes in Central Mexico. J. Volcanol. Geotherm. Res. 197 (1–4), 225–238.

Kessel, R., Schmidt, M.W., Ulmer, P., Pettke, T., 2005. Trace element signature of subduction zone fluids, melts and supercritical liquids at 120–180 km depth. Nature 437, 724–727.

Kim, Y., Miller, M.S., Pearce, F., Clayton, R.W., 2012. Seismic imaging of the Cocos plate subduction zone system in Central Mexico. Geochem. Geophys. Geosyst. 13 (7) https://doi.org/10.1029/2012GC004033.

Kshirsagar, P., Siebe, C., Guilbaud, M.N., Salinas, S., Layer, P.W., 2015. Late Pleistocene Alberca de Guadalupe maar volcano (Zacapu basin, Michoacán): Stratigraphy, tectonic setting, and paleo-hydrogeological environment. J. Volcanol. Geotherm. Res. 304, 214–236.

LaGatta, A., 2003. Arc Magma Genesis in the Eastern Mexican Volcanic Belt. PhD thesis,. Columbia University, New York.

Larrea, P., Salinas, S., Widom, E., Siebe, C., Abbitt, R.J.F., 2017. Compositional and volumetric development of a monogenetic lava flow field: the historical case of Paricutin (Michoacán, Mexico). J. Volcanol. Geotherm. Res. 348, 36–48.

Larrea, P., Siebe, C., Juárez-Arriaga, E., Salinas, S., Ibarra, H., Böhnel, H., 2019a. The ~AD 500–700 (late Classic) El Astillero and El Pedregal volcanoes (Michoacán, Mexico): a new monogenetic cluster in the making? Bull. Volcanol. 81 (10), 1–19.

Larrea, P., Widom, E., Siebe, C., Salinas, S., Kuentz, D., 2019b. A re-interpretation of the petrogenesis of Paricutin volcano: Distinguishing crustal contamination from mantle heterogeneity. Chem. Geol. 504, 66–82.

Larrea, P., Albert, H., Ubide, T., Costa, F., Colás, V., Widom, E., Siebe, C., 2021. From explosive vent opening to effusive outpouring: mineral constraints on magma dynamics and timescales at Paricutin monogenetic volcano. J. Petrol. 62 (4), egaa112.

Lawlor, P.J., Ortega-Gutiérrez, F., Cameron, K.L., Ochoa-Camarillo, H., López, R., Sampson, D.E., 1999. U–Pb geochronology, geochemistry, and provenance of the Grenvillian Huiznopala gneiss of eastern Mexico. Precambriam Research 94, 73–99.

Le Bas, M.J., Le Maitre, R.W., Streckeisen, A., Zanettin, B., IUGS Subcommission on the Systematics of Igneous Rock, 1986. A chemical classification of volcanic rocks based on the Total Alkali-silica diagram. J. Petrol. 27 (3), 745–750.

Legrand, D., Perton, M., Macías, J.L., Siebe, C., Pacheco, J., Chacón, F., Lermo, J., Quintanar, L., Cisneros, G., 2023. Repeated seismic swarms near Paricutin volcano: precursors to the birth of a new monogenetic volcano in the Michoacán-Guanajuato volcanic field, México? Bull Volcanol. 85, 30. https://doi.org/10.1007/s00445-023-01645-0.

Luhr, J.F., 2001. Glass inclusions and melt volatile contents at Parícutin Volcano, Mexico. Contrib. Mineral. Petrol. 142, 261–283.

Luhr, J., Carmichael, I., 1985. Jorullo volcano, Michoacán, Mexico (1759–1774): the earliest stages of fractionation in calc-alkaline magmas. Contrib. Mineral. Petrol. 90, 142–161.

Luhr, J.F., Simkin, T., 1993. Paricutin: The Volcano Born in a Mexican Cornfield. Geoscience Press, 427 pp.

Luhr, J.F., Kimberly, P., Siebert, L., Aranda-Gómez, J.J., Housh, T.B., Kysar Mattietti, G., 2006. México's Quaternary volcanic rocks: insights from the MEXPET petrological and geochemical database. Geol. Soc. Am. Spec. Pap. 402, 1–44.

Mahgoub, A.N., Böhnel, H., Siebe, C., Salinas, S., Guilbaud, M.N., 2017a. Paleomagnetically inferred ages of a cluster of Holocene monogenetic eruptions in the Tacámbaro-Puruarán area (Michoacán, México): implications for volcanic hazards. J. Volcanol. Geotherm. Res. 347, 360–370.

Mahgoub, A.N., Böhnel, H., Siebe, C., Chevrel, M.O., 2017b. Paleomagnetic study of El Metate shield volcano (Michoacán, Mexico) confirms its monogenetic nature and young age (~1250 CE). J. Volcanol. Geotherm. Res. 336, 209–218.

Mahgoub, A.N., Reyes-Guzmán, N., Böhnel, H., Siebe, C., Pereira, G., Dorison, A., 2018. Paleomagnetic constraints on the ages of the Holocene Malpaís de Zacapu lava flow eruptions, Michoacán (Mexico): implications for archeology and volcanic hazards. The Holocene 28 (2), 229–245.

McBirney, A.R., Taylor, H.P., Armstrong, R.L., 1987. Paricutin re-examined: a classic example of crustal assimilation in calc-alkaline magma. Contrib. Mineral. Petrol. 95, 4–20.

Meisel, T., Walker, R.J., Irving, A.J., Lorand, J.P., 2001. Osmium isotopic compositions of mantle xenoliths: a global perspective. Geochim. Cosmochim. Acta 65 (8), 1311–1323.

Meisel, T., Walker, R.J., Morgan, J.W., 1996. The osmium isotopic composition of the primitive upper mantle. Nature 383, 517.
Morelli, S., Garduño Monroy, V.H., Gigli, G., Falorni, G., Arreygue Rocha, E., Casagli, N., 2010. The Tancitaro debris avalanche: characterization, propagation and modeling. J. Volcanol. Geotherm. Res. 193, 93–105.
Németh, K., Kereszturi, G., 2015. Monogenetic volcanism: personal views and discussion. Int. J. Earth Sci. 104, 2131–2146.
Osorio-Ocampo, S., Macías, J.L., Pola, A., Cardona-Melchor, S., Sosa-Ceballos, G., Garduño-Monroy, V.H., Benowitz, J., 2018. The eruptive history of the Pátzcuaro Lake area in the Michoacán Guanajuato Volcanic Field, Central México: Field mapping, C-14 and 40Ar/39Ar geochronology. J. Volcanol. Geotherm. Res. 358, 307–328.
Ownby, S.E., Lange, R.A., Hall, C.M., Delgado-Granados, H., 2011. Origin of andesite in the deep crust and eruption rates in the Tancítaro–Nueva Italia region of the central Mexican arc. Geol. Soc. Am. Bull. 123 (1–2), 274–294.
Patino, L.C., Carr, M.J., Feigensen, M.D., 2000. Local and regional variations in central American arc lavas controlled by variations in subducted sediment input. Contrib. Mineral. Petrol. 138, 265–283.
Pinkerton, H., Wilson, L., 1994. Factors controlling the lengths of channel-fed lava flows. Bull. Volcanol. 56, 108–120.
Pola, A., Macías, J.L., Garduño-Monroy, V.H., Osorio-Ocampo, S., Cardona-Melchor, S., 2014. Successive collapses of the El Estribo volcanic complex in the Pátzcuaro Lake, Michoacán, Mexico. J. Volcanol. Geotherm. Res. 289, 41–50.
Rasoazanamparany, C., Widom, E., Siebe, C., Guilbaud, M.N., Spicuzza, M.J., Valley, J. W., Salinas, S., 2016. Temporal and compositional evolution of Jorullo volcano, Mexico: implications for magmatic processes associated with a monogenetic eruption. Chem. Geol. 434, 62–80.
Reyes-Guzmán, N., Siebe, C., Chevrel, M.O., Guilbaud, M.-N., Salinas, S., Layer, P., 2018. Geology and radiometric dating of Quaternary monogenetic volcanism in the western Zacapu basin (Michoacán, México): implications for archeology and future hazard evaluations. Bull. Volcanol. 80, 18.
Rowe, M.C., Peate, D.W., Ukstins Peate, I., 2011. An investigation into the nature of the magmatic plumbing system at Paricutin volcano, Mexico. J. Petrol. 52 (11), 2187–2220.
Rowland, S.K., Jurado-Chichay, Z., Ernst, G., Walker, G.P.L., 2009. Pyroclastic deposits and lava flows from the 1759–1774 eruption of El Jorullo, Mexico: Aspects of 'violent Strombolian' activity and comparison with Paricutín. In: Thordarson, T., Self, S., Larsen, G., Rowland, S.K., Hoskuldsson, A. (Eds.), Studies in Volcanology, vol. 2. Special Publication of IAVCEI, pp. 105–128.
Rudnick, R.L., Gao, S., 2003. The composition of the continental crust. In: Rudnick, R.L., Holland, H.D., Turekian, K.K. (Eds.), Treatise on Geochemistry - the Crust. Elsevier, Oxford, pp. 1–64.
Salters, V.J.M., Stracke, A., 2004. Composition of the depleted mantle. Geochem. Geophys. Geosyst. 5 https://doi.org/10.1029/2003GC000597.
Schaaf, P., Heinrich, W., Besch, T., 1994. Composition and Sm–Nd isotopic data of the lower crust beneath San-Luis-Potosi, Central Mexico - evidence from a granulite facies xenolith suite. Chem. Geol. 118, 63–84.
Schmidt, M.W., Poli, S., 1998. Experimentally based water budgets for dehydrating slabs and consequences for arc magma generation. Earth Planet. Sci. Lett. 163, 361–379.
Siebe, C., Rodríguez-Lara, V., Schaaf, P., Abrams, M., 2004. Geochemistry, Sr-Nd isotope composition, and tectonic setting of Holocene Pelado, Guespalapa and Chichinautzin scoria cones, south of Mexico City. J. Volcanol. Geotherm. Res. 130, 197–226.
Sosa-Ceballos, G., Emmanuel Boijseauneau-Lopez, M., Daniel Perez-Orozco, J., Cifuentes-Nava, G., Bolos, X., Perton, M., Simon-Velazquez, D., 2021. Silicic magmas in the Michoacan-Guanajuato volcanic field: an overview of plumbing systems, crustal storage, and genetic processes. Revista Mexicana de Ciencias Geológicas 38 (3), 210–225.
Stracke, A., Bourdon, B., 2009. The importance of melt extraction for tracing mantle heterogeneity. Geochim. Cosmochim. Acta 73 (1), 218–238.
Straub, S.M., Gómez-Tuena, A., Zellmer, G.F., Cai, M.Y., Goldstein, S.L., Langmuir, C.H., Espinasa-Pereña, R., 2008. Petrogenesis of alkaline arc basaltic andesites at Volcan Chichinautzin in the Central Mexican Volcanic Belt. Geochim. Cosmochim. Acta 72 (12), A906.
Straub, S.M., Gómez-Tuena, A., Zellmer, G.F., Espinasa-Perena, R., Stuart, F.M., Cai, Y., Langmuir, C.H., Martin-Del Pozzo, A., Mesko, G.T., 2013. The processes of melt differentiation in arc volcanic rocks: insights from OIB-type arc magmas in the central Mexican Volcanic Belt. J. Petrol. 54, 665–701.
Straub, S.M., Gómez-Tuena, A., Bindeman, I.N., Bolge, L.L., Brandl, P.A., Espinasa-Pereña, R., Solari, L., Stuart, F.M., Vannucchi, P., Zellmer, G.F., 2015. Crustal recycling by subduction erosion in the central Mexican Volcanic Belt. Geochim. Cosmochim. Acta 166, 29–52.
Sun, S.S., McDonough, W.F., 1989. Chemical and isotopic systematics of oceanic basalts: implications for mantle composition and processes, Magmatism in the ocean basins. Geol. Soc. Lond. Spec. Publ. 42, 313–345.
Torres-Sánchez, D., Sosa-Ceballos, G., Bolós, X., Macias, J.L., 2022. Petrogenesis of mafic-intermediate magmatism of the Michoacán-Guanajuato Volcanic Field in western Mexico. A geochemical review. Front. Earth Sci. 1569.
Valentine, G.A., Connor, C.B., Mcnutt, S., 2015. Basaltic volcanic fields. In: Sigurdsson, H., Houghton, B.F., Rymer, H., Stix, J. (Eds.), The Encyclopedia of Volcanoes, 2nd edition, pp. 423–439.
Verma, S.P., 2000. Geochemistry of the subducting Cocos plate and the origin of subduction unrelated mafic volcanism at the front of the central Mexican Volcanic Belt. In: Delgado-Granados, H., Aguirre-Díaz, G., Stock, J. (Eds.), Cenozoic Tectonics and Volcanism of Mexico, Geological Society of America Special Paper, vol. 334, pp. 1–28.
Verma, S.P., Hasenaka, T., 2004. Sr, Nd, and Pb isotopic and trace element geochemical constraints for a veined-mantle source of magmas in the Michoacán-Guanajuato volcanic field, west-central Mexican Volcanic Belt. Geochem. J. 38 (1), 43–65.
Vervoort, J.D., Patchett, P.J., Albarède, F., Blichert-Toft, J., Rudnick, R., Downes, H., 2000. Hf–Nd isotopic evolution of the lower crust. Earth Planet. Sci. Lett. 181 (1–2), 115–129.
Wilcox, R.E., 1954. Petrology of Parícutin Volcano Mexico. In: U.S. Geological Survey Bulletin 965C, pp. 281–353.
Workman, R.K., Hart, S.R., 2005. Major and trace element composition of the depleted MORB mantle (DMM). Earth Planet. Sci. Lett. 231, 53–72.